Ecological Informatics 88 (2025) 103127

Contents lists available at ScienceDirect

Ecological Informatics

journal homepage: www.elsevier.com/locate/ecolinf

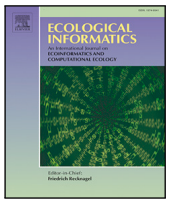

Forest variables from LiDAR: Drone flight parameters impact the detection of tree stems and diameter estimates

Paul M. Eisenschink *, Wolfgang A. Obermeier, Vinzenz H.D. Zerres, Annika M. Suerbaum, Lukas W. Lehnert

Department of Geography, Ludwig-Maximilians-Universität, Luisenstr. 37, 80333, Munich, Germany

ARTICLE INFO

Dataset link: https://data.mendeley.com/datasets/5fjwb9hfpm/1

Keywords:
UAV LiDAR remote sensing
Forest management
Point cloud segmentation
Stem diameter estimation

ABSTRACT

Ecosystem services provided by central European forests, often dominated by Norway spruce or Scots pine, are increasingly threatened by climate change. Monitoring, while labour intensive, is key to ensure continuing forest health. Consequently, UAV-based LiDAR remote sensing has become a valuable tool. However, the impact of drone flight parameters on LiDAR data quality has not yet been extensively studied. To address this, we first present a methodology for delineating tree stems, estimating their diameter at breast height (DBH), and separating understory vegetation from stems and old-grown trees to subsequently compare the approach to other existing methods. Second, we analyse how drone flight parameters influence the accuracy of forest parameter detection. Our methodology outperformed existing approaches in stem detection and DBH estimation. Understory detection enabled the identification of forest paths, roads, and areas without understory vegetation. Differences in flight parameters had a large effect on the accuracy of the approach. Optimal data usability was achieved by flying the drone at low flight height above the trees, at relatively high speeds, and with high LiDAR stripe overlap, balancing detailed data collection with efficient area coverage. We conclude that the new approach can provide foresters with detailed insights into forest structure and dynamics, reducing the need for extensive fieldwork.

1. Introduction

Forests worldwide provide crucial ecosystem services, such as carbon storage (Fahey et al., 2009), recreational and cultural services (Brockerhoff et al., 2017), or the provision of timber (Zhang et al., 2020). Mostly for the latter reason, commercially used forests in Central Europe are often dominated by Norway spruce (*Picea abies*) and Scots pine (*Pinus sylvestris*) (Brandl et al., 2020), as they grow relatively fast and can therefore provide timber on a large scale (Caudullo et al., 2016; Pyhäjärvi et al., 2019). The economic yield of spruce and pine trees is increasingly threatened because climate change negatively impacts tree health (Brandl et al., 2020). Consequently, the frequency and magnitudes of forest disturbances are increasing in Central Europe (Caudullo et al., 2016, Dyderski et al., 2018). The drought in the years 2018 to 2020 demonstrated the high susceptibility to disturbances of spruce-dominated forests, causing forest losses of nearly 5000 km^2 in the regions of the Harz, Thuringian Forest, and the Erz mountains in central Germany (Thonfeld et al., 2022). Future projections show that the frequency and intensity of drought events will increase, accelerating the pressure on the remaining spruce-dominated forests and most likely increasing disturbances in previously less affected areas such as forests in southern Germany (Huang et al., 2015; Spinoni et al., 2018; Kloos et al., 2021; Poschlod et al., 2020).

With increasing economic and ecological demands and intensifying threats from disturbances, foresters are forced to apply measurements to foster resistance and resilience in their forests. To analyse the effect of pre-calamity measures, a dense monitoring network is required, which is time-consuming if performed in situ. An alternative method to obtain the necessary information about forest health and change in forest structure is the use of high resolution airborne LiDAR scanners (ALS, Campbell and Wynne, 2011). This method, often powered by unmanned aerial vehicles (UAV), has been proven to be capable of detecting individual trees and obtaining important tree parameters such as tree height and crown area (Ferraz et al., 2016). Regarding economic and ecological values of trees, stem diameter is a crucial variable, which, however, remains difficult to derive from ALS data alone. In contrast, several approaches of estimating tree parameters such as stem diameter, volume, etc. (Singh et al., 2022) have been developed for terrestrial LiDAR data (TLS, Corte et al., 2020). Among the available approaches for ALS, Chisholm et al. (2013) were among the first to

* Corresponding author.
E-mail address: p.eisenschink@lmu.de (P.M. Eisenschink).

https://doi.org/10.1016/j.ecoinf.2025.103127
Received 9 December 2024; Received in revised form 27 February 2025; Accepted 1 April 2025
Available online 15 April 2025

Nomenclature

ALS	Airborne Laser Scanning
CHM	Canopy Height Model
DBH	Diameter at Breast Height
DBSCAN	Density-Based Spatial Clustering of Applications with Noise
DTM	Digital Terrain Model
FP	Flight Parameter
H	Flight Height (Flight Parameter)
HDBSCAN	Hierarchical Density-Based Spatial Clustering of Applications with Noise
LiDAR	Light Detection and Ranging
LMU	Ludwig Maximilian University
NRMSE	Normalised Root Mean Square Error
O	Overlap of LiDAR Stripes (Flight Parameter)
PCA	Principal Component Analysis
PLS	Portable Laser Scanning
S	Flight Speed (Flight Parameter)
TLS	Terrestrial Laser Scanning
UAV	Unmanned Aerial Vehicle

develop basic methods for estimating stem diameter. However, their algorithm failed to detect most of the trees, especially if they stood far from the central flight line. Brede et al. (2017) compared stem diameters from manually segmenting the stem points from ALS data to that of TLS data and found a similar precision. They concluded that ALS data recording for stem detection is more time efficient compared to TLS data retrieval. Building upon the method of Chisholm et al., 2013, Neuville et al., 2021 described an algorithm for ALS data to segment the bole area of trees in the segment relevant to the vital parameter of stem diameter at breast height (DBH, Ter-Mikaelian and Korzukhin, 1997) and automatically estimate stem diameter. Their approach first performs individual tree segmentation and then tries to delineate the stem of each tree. Consequently, if individual tree detection fails to separate the canopy into trees, the stem detection algorithm will miss the corresponding stems.

A critical issue regarding the detection of stems using ALS under close canopies is that stems can only be detected if enough LiDAR beams are reflected off the stems, resulting in a high 3D point cloud density in the stem segment. This depends mainly on the choice of flight parameters, such as flight speed and flight height. Since so far research on stem detection and stem diameter estimation did not investigate these effects (Neuville et al., 2021; Brede et al., 2017; Liao et al., 2022; Chisholm et al., 2013), we initially performed a systematic comparison of stem detection accuracy and stem diameter calculation for different forest stands. Beside applying these two existing approaches (Neuville et al., 2021, de Conto et al., 2021), we present an enhanced version of the approach developed by Neuville et al. (2021), which directly detects the stems without the need to identify individual trees first. Based on this new approach, we hypothesise that we can increase the accuracy of stem detection.

In particular, this paper will initially aim to find an ideal set of flight parameters for low-cost UAV based LiDAR remote sensing, with a focus on the stem segment of trees. Secondly, an adapted algorithm to delineate stem points from a dense 3D point cloud will be described to enable faster tree segmentation over larger areas. Lastly, a method for the estimation of DBH based on these segmented stems will be presented, and the capabilities of both methods are compared to previous work in the field.

2. Materials and methods

2.1. Study area

The study has been conducted in a managed forest located near the city of Landshut in southern Germany. This region shows annual average precipitation of 859 mm and a yearly average temperature of 9.1 °C (Deutscher Wetterdienst (DWD), 2024). The experimental sites for this study cover 9 ha of the forest owned by the Ludwig-Maximilians-University of Munich (LMU) (Fig. 1).

The mixed forest in the study area consists of approximately 65 % coniferous and 35 % broadleaf trees, with the main tree species being Norway spruce (*Picea abies*), Scots pine (*Pinus sylvestris*) and Beech (*Fagus sylvatica*). The site is dominated by a small stream that stretches in a north-easterly direction, with slopes towards the creek. The maximum tree height is around 42 m with some younger and lower tree stands with heights around 15 to 20 m. The tree stand density shows a large variability for some areas, as does the forest stand age, ranging from some old spruce and pine trees with an age of around 80 years, while around 30 years younger stands of broadleaf trees can be found to the north. Similarly, the presence and density of understory vegetation varies largely, with height ranges from around 0.5 m to 12 m, consisting mainly of planted beech and spruce trees.

The study area was specifically chosen for its heterogeneous forest structure, with four subplots of varying characteristics were selected to assess the performance methods' performance over a wide range of forest structural parameters. The four subplots mainly consist of old-growth conifers (spruce and pine) both with little to no advanced regeneration (1), very dense advanced regeneration of beech up to 10 m in height (2), old-growth broadleaf trees (oak, beech, and maple) with a decent amount of advanced regeneration up to 4 m (3), and younger coniferous trees (4) and are around 0.1 ha in size (compare Fig. 2 for a canopy height model (CHM) with subplot locations and a digital terrain model (DTM), both derived from UAV-LiDAR data).

2.2. Field work

To analyse the impact of flight parameters (FPs) on data accuracy and usability of LiDAR remote sensing, eight flights with different combinations of flight height (abbreviated as H in the names of the flights in the following), speed (S), and side overlap of LiDAR stripes (O) have been conducted in May and July 2024 (Table 1) during days with low wind speeds and no precipitation (a schematic overview of different FPs is shown in Fig. 3). To check for differences between day- and nighttime data, an additional flight was conducted in July at night. All flights were performed in a double grid manner to increase point density and to allow observations from multiple directions (Swayze et al., 2021).

A total of 148 trees were selected within the study area to validate the LiDAR-derived tree parameters. The trees were chosen to represent the differing forest stands and tree species found within the forest. Of the total selected trees, 72 are used for training and 76 for validation. Of the latter, 30 are spread over the entire study area, and 46 within the four subplots. For each tree, the location has been determined with a differential GPS (StoneX S850 A) and diameter at breast height (DBH) values were recorded for each tree using a standard tree calliper. The tree heights range from 5 to 40 m and show a DBH between 6 to 74 cm (compare Appendix Fig. A.1 for the measured DBH-values for the entire study area as well as the subplots).

2.3. LiDAR algorithms

2.3.1. Data collection and preparation

LiDAR data was recorded using a Geosun GS-100C+ LiDAR Scanner (Wuhan Geosun Navigation Technology Co., Ltd) on a DJI Matrice M300 Drone (SZ DJI Technology Co., Ltd.). Using Geosun's software

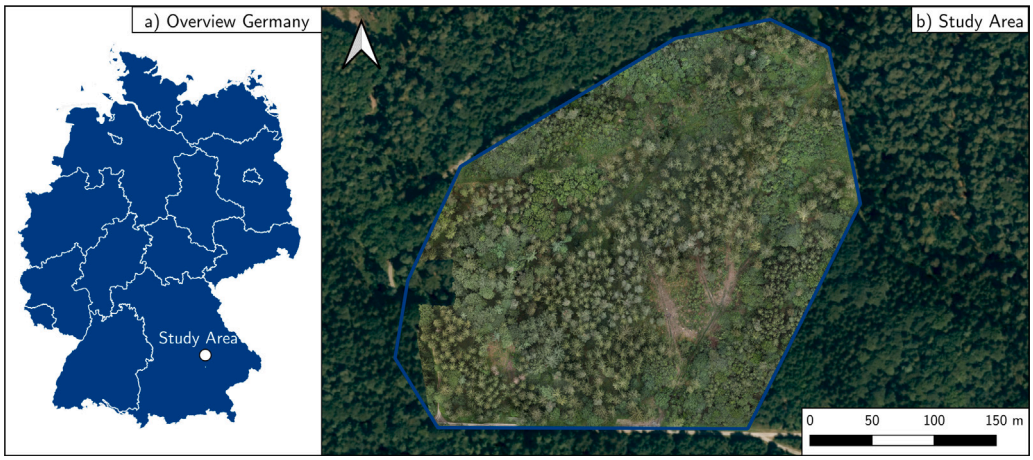

Fig. 1. Overview of the study area, with (a) the position of the study area in Germany, and (b) an orthophoto of the forest in the study area.

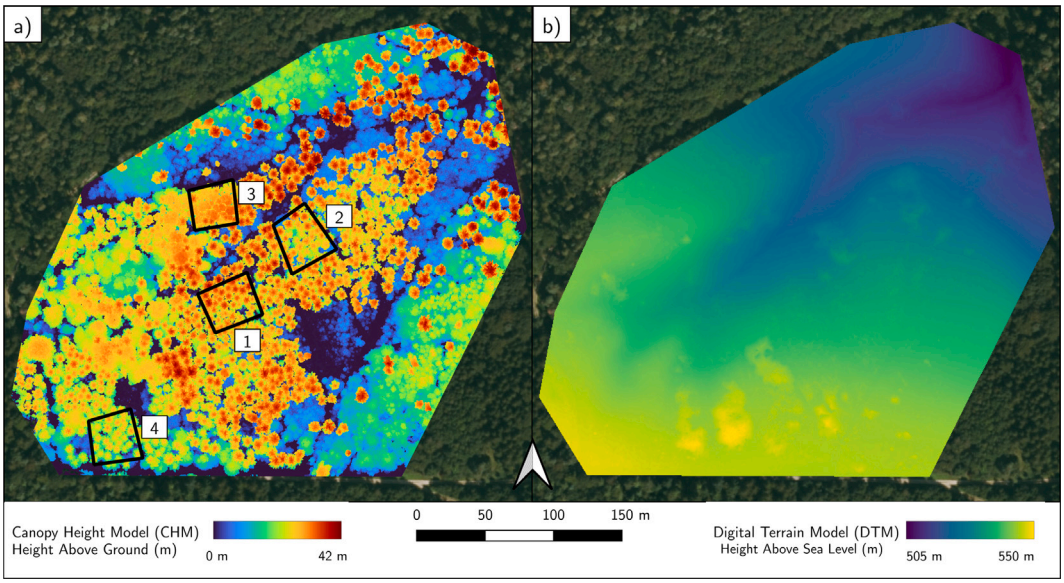

Fig. 2. Canopy height model (CHM; a) and digital terrain model (DTM; b) of the study area based on LiDAR data. CHM shows recent felling of trees (mainly within the dark blue areas) as well as subplots of differing forest structure for later analysis, while DTM gives overview of the terrain. The subplots consist of two old-growth conifer stands without (1) and with dense understory vegetation of beech (2), a close-canopied stand of old-growth broadleaf trees (3), and a stand of dense, but younger conifers (4). (For interpretation of the references to colour in this figure legend, the reader is referred to the web version of this article.)

Table 1
Table of flight parameter (FP) sets and basic point cloud metrics thereof.

Height	Speed	Overlap	Time	Date	Name of FP set	Point density	Ground points
50 m	6.0 m/s	30%	Day	2024–05–15	H50 S60 O30	2160.1 Pts/m^2	13.8%
50 m	6.0 m/s	45%	Day	2024–05–21	H50 S60 O45	2705.5 Pts/m^2	14.4%
50 m	6.0 m/s	60%	Day	2024–05–16	H50 S60 O60	3826.3 Pts/m^2	14.6%
70 m	6.0 m/s	30%	Day	2024–05–15	H70 S60 O30	1514.6 Pts/m^2	15.1%
90 m	6.0 m/s	30%	Day	2024–05–15	H90 S60 O30	1022.0 Pts/m^2	17.4%
50 m	4.0 m/s	30%	Day	2024–05–15	H50 S40 O30	3119.2 Pts/m^2	13.7%
50 m	5.0 m/s	30%	Day	2024–05–15	H50 S50 O30	2617.6 Pts/m^2	13.9%
50 m	6.0 m/s	30%	Night	2024–07–02	H50 S60 O30 N	2133.9 Pts/m^2	14.6%

shipped with the device (version 6.2 for the trajectory calculation and 5.0 for the point cloud generation), flight-data were processed, and LiDAR stripes were stitched together. The resulting point cloud was then checked for offsets using ground targets, and height-normalised by transforming the height values of all points to above ground, instead of above sea level. Ground segmentation was performed with the lidR-package (Roussel et al., 2020) using the cloth simulation function (CSF) (Zhang et al., 2016) in CRAN R. Finally, each of the eight datasets retrieved under the respective FP set were clipped using the same area outline as seen from the study area overview, to ensure comparability between the datasets.

2.3.2. Stem delineation algorithm

Three different algorithms for stem detection and/or DBH estimation have been compared. The first one was developed by de Conto et al. (2017) for TLS data, but can be also applied to ALS data (de Conto,

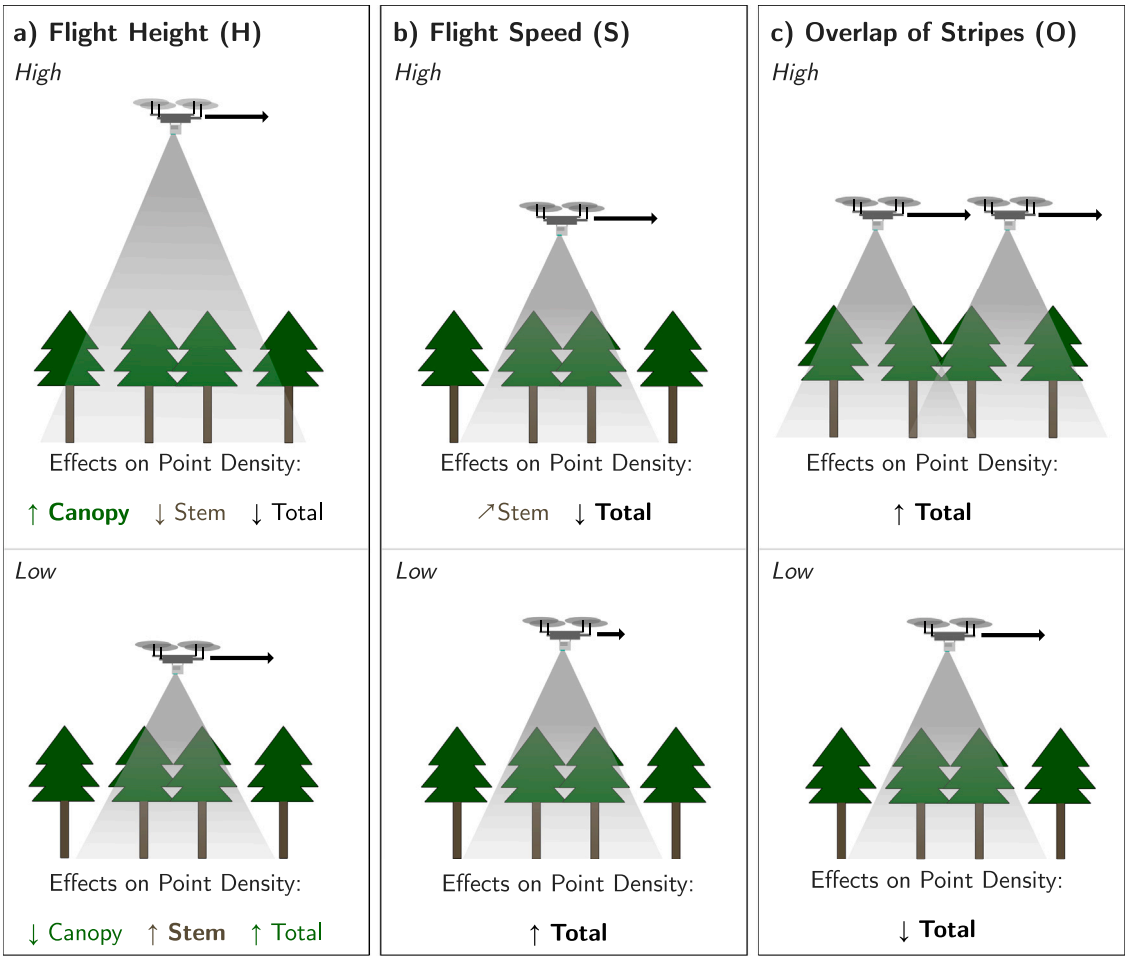

Fig. 3. Conceptual visualisation of effects of flight parameters flight height (a), speed (b), and overlap (c) on Lidar point clouds of UAV flight parameters and their influence on point density for the canopy, and stem segment, as well as for total point density. Examples for high values in the first row, low values in the second row.

2020). The second one has been developed for a deciduous forest in Western Germany utilising ALS data acquired with a similar system to that used in this study (Neuville et al., 2021). Using the concept of Neuville et al. (2021), we developed a third approach, which uses a sliding window instead of a tree-wise approach. In the following, each algorithm will be briefly explained:

TreeLS's method of segmenting the stems functions via Hough-transformation (Fig. 4a). After an initial segmentation of individual trees by clustering points based on spatial proximity, the point cloud of each tree is sliced vertically every 0.5 m. For each slice, a Hough-transformation is used to detect circles. If multiple circles were found vertically stacked above each other starting from a defined base height, the method detects these points as part of a stem, labelling the points accordingly (de Conto et al., 2017).

The DBH estimation algorithm by Neuville et al. (2021) technically does not provide a segmentation of entire stems as an intermediate product, but rather uses the detected parts of stems at breast height for DBH estimation directly (Fig. 4b). This method functions on individually segmented trees, clustering the bottom third of the tree points per height using HDBSCAN (Campello et al., 2013), while disregarding the Z-variable. The algorithm then iteratively reduces the minimum point number for a cluster to be labelled as such until the cluster satisfies the conditions of realistic diameter (below 1.5 m), minimum vertical length, and vertical continuity. This is then defined as the cluster of points that represent the stem segment. The cluster is then cut to the extraction interval between 1.2 and 1.4 m and the DBH is estimated via a circle fit checking for different growth directions via a principal component analysis (PCA). The original parameter set used by Neuville et al. (2021) provided only a small number of stems and corresponding DBH values for the present study site. Therefore, the height segment of the stem at which points are used to estimate the DBH (originally between 1.2 & 1.4 m) has been set between 1 and 3 m. Additionally, the starting minimum number of cluster points for the HDBSCAN was reduced to speed up computation.

The newly developed stem delineation algorithm did not rely on the detection of individual trees like the precursor algorithm by Neuville et al. (2021) (Fig. 4c), as the segmentation of individual trees in ALS data can be error-prone, often leading to over- or under-segmentation of individual trees (Jeronimo et al., 2018). Therefore, we split the point cloud into quadratic cells of a chosen size (e.g., 20 by 20 m), iterating over every cell individually. We have found that higher cell sizes increase the amount of physical memory necessary for calculation, while shortening computing time. To exclude ground below 0.5 m and canopy points above 15 m, the delineation only regards the relevant height segment for the stems (e.g., between 0.5 and 15 m). This segment is then initially clustered using HDBSCAN, only regarding X- and Y-variable of the points, similar to the original method. This is done as stems are assumed to be more or less straight and should be represented by dense clusters of vertically stacked points. To differentiate between stems and other objects, a PCA is performed for each cluster. Subsequently, it is checked if the following four conditions, which are adapted compared to the original method, are met (note that all these parameters can be adapted to work for other LiDAR systems and study areas, but were found to produce the most accurate segmentation of stems for our data):

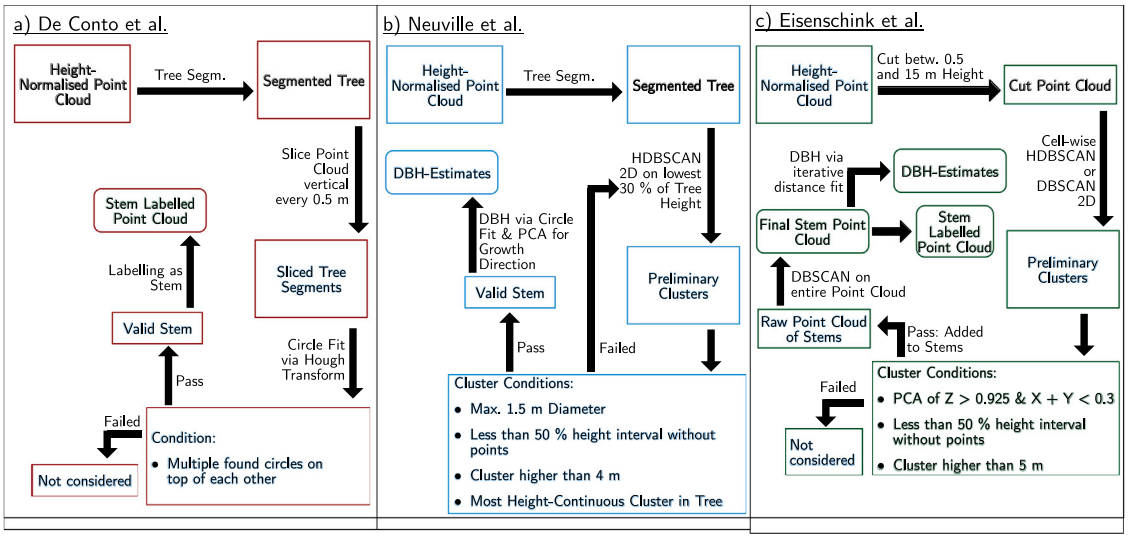

Fig. 4. Flow-chart of applied methods by de Conto et al. (2017) (a) and Neuville et al. (2021) (b), as well as the newly developed algorithm (c).

1. The principal component associated with the Z-direction explains at least 92.5% of the variance.
2. The principal components for the X- and Y-variables explain less than 30 % of the variance in total.
3. The vertical histogram of points with 1 m bins has less than five empty bins, similar to the original method, and the standard deviation of densities is less than 0.8 m (indicating that points are vertically homogeneously distributed).
4. The length of the entire cluster between lowest and highest point of height is more than 5 m.

If a cluster meets all conditions, it is assumed to be a stem and is collected into a new point cloud containing only points of detected stems labelled with tree IDs. Finally, a second round of clustering using DBSCAN (Ester et al., 1996) is performed on the entirety of the detected stems to filter out any remaining noise caused by points from branches or understory vegetation. Compared to HDBSCAN, this clustering method requires additional information on the approximate size of clusters. Due to the previous steps, this is relatively easy, as the remaining clusters of stems are more or less of similar size, compared to remaining points of other sources, like shrubs or other lower vegetation. Additionally, DBSCAN is significantly less computationally demanding, as it does not calculate a point hierarchy like HDBSCAN (Campello et al., 2013), and can therefore be used on all stems at once. Additionally, it combines any falsely segmented stems, if they are located on edges of two cells, while also generating a unique ID for every stem. Finally, the detected stem points are reintegrated into the original point cloud, which contains the points of the detected stems labelled with their stem ID. This is different to the method from Neuville et al. (2021), which is not capable of identifying points of individual tree stems. Note that for very large areas, the first clustering of our method can also be performed using DBSCAN. This requires setting the parameter of cluster size to fit the present stems, but speeds up the calculation substantially. Even more importantly, the usage of DBSCAN significantly reduces memory consumption, as HDBSCAN requires the calculation of the core distance between every point in the point cloud, which non-linearly increases the memory consumption with increasing point clouds (Campello et al., 2013).

2.3.3. Understory detection

Using the stem delineation algorithm, it is further possible to detect the understory vegetation of the forest. Histograms of point heights for this study area revealed a large number of points on the forest floor. From a height of around 2 m upwards, the density of points decreased rapidly and only increased at around 18 to 20 m with the canopy. Removing the detected stem points from the point cloud, a break point separating understory vegetation and canopy can be detected automatically. Hence, a cell-wise calculation (20 m per cell) is performed to detect this break point, by getting the first local minimum of the density of point heights above ground. This ensures that heights of understory vegetation are adapted to the local forest conditions and can differ across the area of investigation. The algorithm creates a raster of this break point for each cell. To counteract the problem caused by very small vegetation not covered by canopy or at the edge of canopies, cells in the raster with a breakpoint below 3 m were increased to 5 m. Finally, to return a point cloud that contains only the understory vegetation, each cell of the point cloud is clipped, removing ground points and points above the calculated break point from the raster.

2.3.4. DBH-estimation

The estimation of DBH iterates over every delineated stem, first clipping the chosen height segment (e.g., between 1 and 2 m). This set of points is then flattened into a 2D-space, ignoring the Z-variable. The DBH is then estimated with an iteratively adopted quantile of the total amount of distances between every point within the 2D-space. The iterative selection of the quantile is performed together with the selection of other parameters described below. Finally, the centre X- and Y- coordinates, the estimated DBH in cm, and ID of every stem are stored. As the DBH estimation requires the setting of the three additional parameters (1) the quantile of estimation, (2) the upper, and (3) the lower height segment of extraction, an iterative method for maximising the accuracy was developed. Using the training dataset, this method cycles through the three parameters and compares the results of the algorithm to the measured stems by local join, recording recall of stems compared to the measured ones, the adjusted R^2, and normalised RMSE of the diameter estimation, using the min–max method for calculation. The validation set is then used to validate the optimisation, as are the measured DBH-values within the four subplots.

3. Results

3.1. Flight parameters

The selection of flight parameters influenced point densities and the number of return points at the ground (Table 1). Lower flight speeds and higher overlaps resulted in higher point densities and a higher number of total points over the entire study area. Percentage of points returned from the ground increased with flight height, but was only

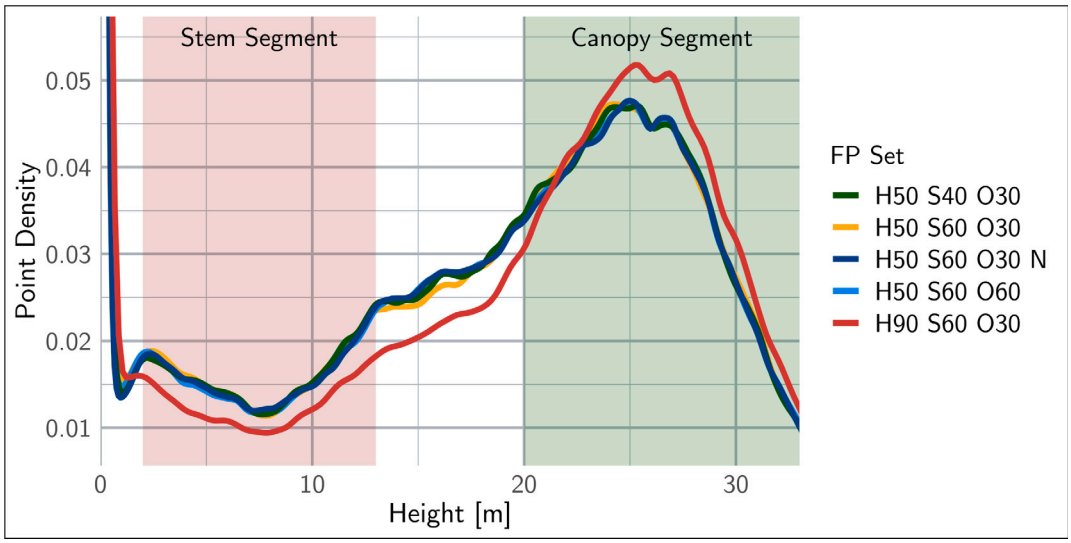

Fig. 5. Point density distributions for the most relevant flight parameter (FP) sets with stem and canopy segment denoted. For the absolute number of points see Table 1.

marginally affected by altered speeds and overlaps. Intermediate values of FP parameters, meaning for example an overlap of 45% or flight height of 70 m, led to intermediate point densities and percentages of reflected ground points. Consequently, we focus on the flights conducted with extreme values of FP in the following and describe their effects on stem detection and diameter calculation.

The general pattern of point density distributions acquired with different FPs were similar, with large point densities at the ground, lowering in the area of stems (between 2 & 12 m), and increasing again with the canopy (Fig. 5). The first small spike in data at around 1.5 m height was likely caused by the LiDAR's inability to penetrate lower shrubs and grasses, decreasing the number of points underneath. A notable exception was the density of the data retrieved from the highest flight (H90 S60 O30). This data contained fewer points in the stem segment, while those in the canopy increased, with a point of intersection to the other FP sets' data at around 23 m. It can also be seen that the difference between the data with high overlap (H50 S60 O60) and the data acquired at slow speed (H50 S40 O30) was particularly small. Lastly, the FP set using the LiDAR's default settings (H50 S60 O30), shows a slight drop in point density at higher stem heights at around 15 m, while otherwise being quite similar. To analyse the effect of varying forest structure and FP set on the data, the point densities and their distribution in the four subplots were used. Total point densities followed the order of the entire area's dataset, with the densely overlapped and slowest flown data providing the highest point numbers (Table A.2). The point density distributions showed a relatively low impact of the FP sets in the subplots. A comparably strong response in the nightly flown data (H50 S60 O30 N) for the subplots 3 & 4 might be caused by the advanced phenological stage in July. Only subplot 4 showed a higher relative point density at the canopy segment for the densely overlapped data, compared to the other subplots (compare Fig. A.2).

3.2. Stem delineation algorithms

The stem delineation was applied to the five most extreme FP sets as done for the whole study area above and over the four subplots of differing forest structure. Recall, that is, the fraction of stems visible in the LiDAR data versus stems correctly segmented by the algorithm, was highest for densely overlapped data (H50 S60 O60) at around 87 % followed by the slowly flown data (H50 S40 O30), the standard parameter data (H50 S60 O30), the nightly flown data (H50 S60 O30 N), and lastly the high flight height data (H90 S60 O30). Recall in the individual subplots revealed similar trends, giving the densely overlapped data the highest recall in three of the four subplots and second highest in the fourth (For the entire table of recalls per subplots and FP sets see Table A.2.)

As the densely overlapped flight stripes data (H50 S60 O60) proved to be the best FP set for stem remote sensing in terms of recall, the stem delineation algorithms were applied to the data recorded at an overlap of 60% for the next comparison, consisting of a stand of old-growth coniferous trees of up to 43 m (Fig. 6a). Results of stem delineation using TreeLS and the new algorithm differed not only in terms of number of detected stems, but also in terms of the precision of the algorithm to distinguish between stems and branches (Fig. 6b & c). Using TreeLS, only about 70% of stems were detected, while our new algorithm only failed at detecting three out of 30 stems (10%). In addition, while the stem parts close to the tree crowns contained larger horizontal branches if classified with TreeLS, only the vertical parts of the stems were labelled as such with the new algorithm. Over the four subplots, this difference is even larger, giving the new algorithm an average recall of 86.7% and TreeLS a recall of 56.2% (Table A.2.). Since the method from Neuville et al. (2021) does not return segmented stems, no direct comparison is possible to the other methods.

The performance of the algorithm by de Conto et al. (2017) and the new approach have been compared in the four subplots. The average recall in these subplots was 87 % for the newly developed algorithm, while TreeLS' method achieved only 56 %. Especially in the second subplot with dense and relatively high understory vegetation, the new algorithm substantially outperformed TreeLS' method. In areas mainly covered by broadleaf trees, where number of Lidar points at the stems was generally low, both algorithms performed insufficiently, with our method at least delineating some larger broadleaf trees.

Since the new algorithm outperformed TreeLS' method both regarding the recall and delineation accuracy, only the results of the new algorithm are shown for the entire study area (Fig. 6d). Here, the newly designed algorithm detects 4951 stems, resulting in a stem density of around 549 trees per hectare. Using DBSCAN instead of HDBSCAN to initially cluster tree stems also showed good results, with only slight errors of falsely disregarded stem points, while decreasing calculation time for spatially larger point clouds.

The point clusters classified as stems were not always circular. Instead, some stems had elliptic shapes (Fig. 7 c) or were even straight or curved lines (Fig. 7a & f), while some trees are sensed as circles (Fig. 7d & e). The main factor for the 'roundness' of the stem areas seems to be the LiDAR's penetration of canopy or lower vegetation to the stem, giving best results for stems in areas with low advanced regeneration and non-closed canopies. This implies that a circle fit might not be

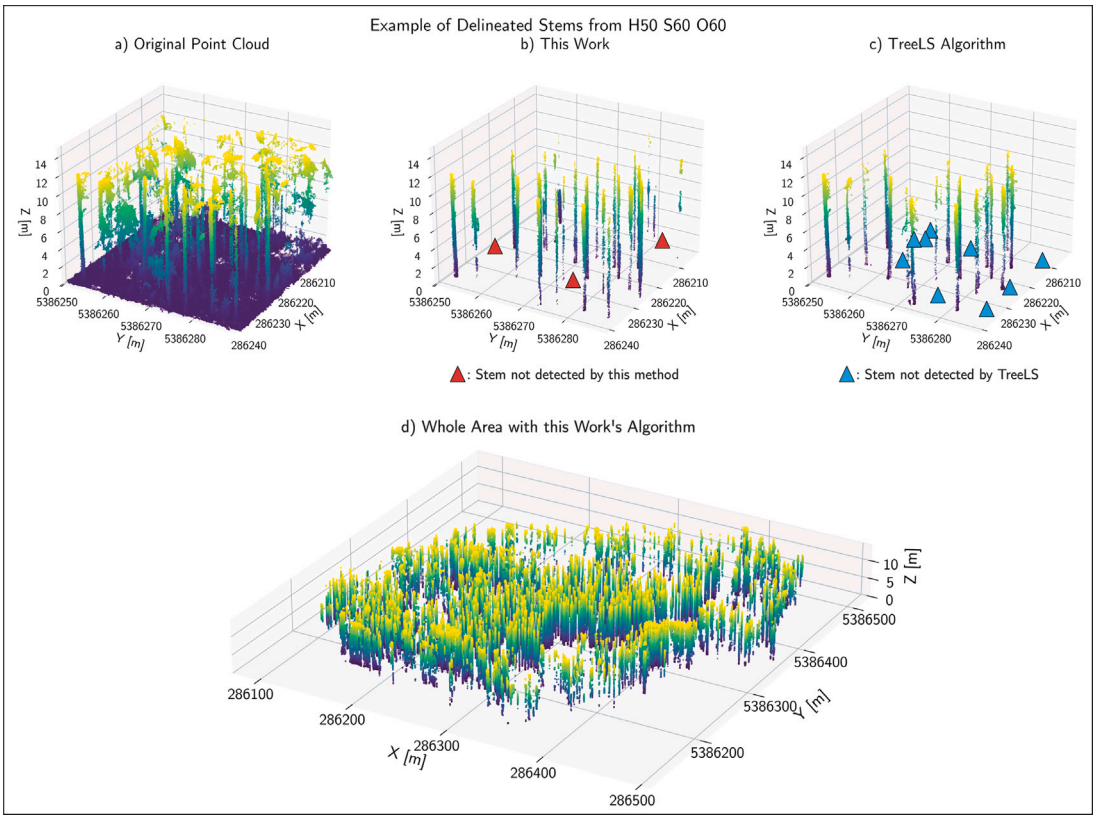

Fig. 6. Subset of study area with original point cloud (a), delineated stems by the new algorithm (b), and TreeLS algorithm for comparison (c) both with missing stems marked by triangles, and stems from the entire study area delineated with the new algorithm (d) all based on the best performing flight parameter (H50 S60 O60). Coordinates are given in UTM zone 33N.

a suitable method for the diameter extraction of every tree. In the cases of curved lines, a circle fit will over-estimate the diameter. One disadvantage of the newly developed as well as TreeLS' method can be seen for trees with very unusual growing direction. This means that the algorithm struggles to segment half-fallen trees or stems that diverge quite low from the ground and at a shallow angle.

3.3. Understory detection

The spatial pattern of understory vegetation reflected the network of forest roads and paths in the area of investigation (Fig. 8a), which is less visible in the RGB data and in the canopy height maps (Fig. 8b). The dense understory vegetation in the centre is mainly composed of broadleaved trees planted approximately 20 years ago, which are considerably higher compared to the rest of the understory vegetation in the area. Some areas not covered by trees near the centre of the study area are also present in the understory data, even though they are not located below any higher trees, therefore they are technically no understory vegetation. Some areas with little understory vegetation are in the south-western part of the study area (Fig. 8a). These areas are comprised of some older conifers and broadleaf trees, underneath which no natural or planted lower vegetation could establish. Similarly, no vegetation was able to grow below a stand of spruce trees of around 20 m height.

Since penetration of the canopy might be higher in spring than in summer, due to less foliage blocking the LiDAR's beam, we further tested whether this affects the accuracy of the detection of understory vegetation in our datasets. Therefore, we compared the canopy maps of understory vegetation for datasets with standard parameters (H50 S60 O30) acquired in May and July. We found very similar patterns, except for some small artefacts at the edge of the study area. Distributions of pixel heights differed marginally between May and July, with more pixels of lower height present in spring, while there were fewer pixels in heights above 8 m (Fig. 8c). Maximum values of both density curves were at 5 m. This is caused by the additional breakpoint setting, putting for every cell with breakpoint below 3 m to 5 m, as described in the methodology.

3.4. DBH-estimation

The iterative tuning method results in values for the heights of extraction, the adjusted R^2s of measured versus estimated DBH, and their normalised RMSE (NRMSE) for every FP set (Fig. 9).

Two flight parameter combinations resulted in substantially higher R^2 values compared to the others: The highest flown data (H90 S60 O30) at an extraction height for the DBH at 1 m and the densely overlapped H50 S60 O60 at 2.5 m, with the latter showing a considerably lower NRMSE than the other FP combinations (compare Fig. 9b). Noteworthy, the high adj. R^2 for H90 S60 O30 stems might be a consequence of the low number of stems in this dataset. We therefore conclude that an estimation of DBHs with data from H50 S60 O60 at a stem height of 2.5 $\pm$ 0.5 m is most accurate, while also providing the highest recall of individual stems compared to those measured at 36%, representing the percentage of detected stems with enough points to robustly calculate a diameter compared to the total number of detected stems. The scatter plot between measured and estimated DBH values of this FP set is shown in Fig. 9c, scatter plots for the other FP sets can be found in Fig. A.3.)

To further analyse the dependence in the DBH estimation's performance on different forest structure, we tested DBH estimation in the four subplots, and for the five most extreme FP sets. Note, that the trees were selected for measuring, if they were successfully estimated by the DBH algorithm for at least one FP set and are therefore not randomly chosen, like the training data. The best performance in both recall and

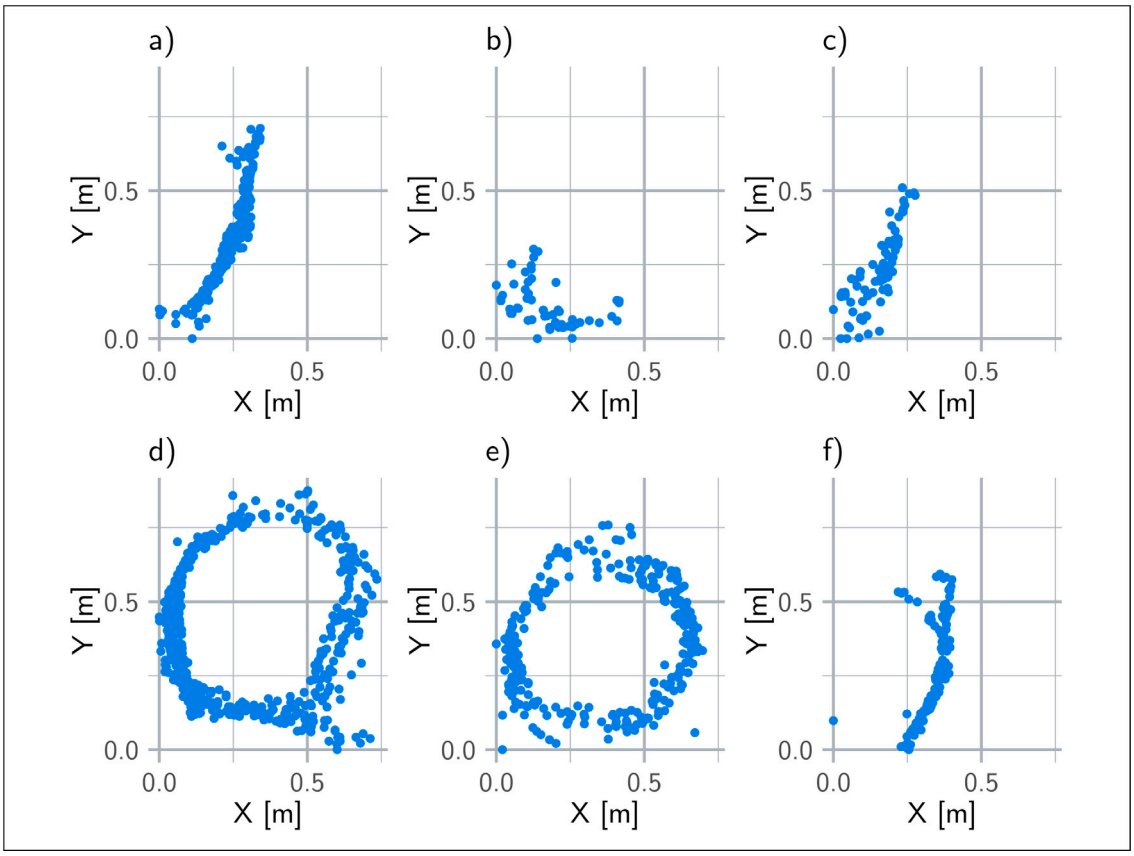

Fig. 7. Examples of cross sections of stems between 0.5 and 2 m above ground. The stems have been detected using the new algorithm showing differences in shapes of stems in the data.

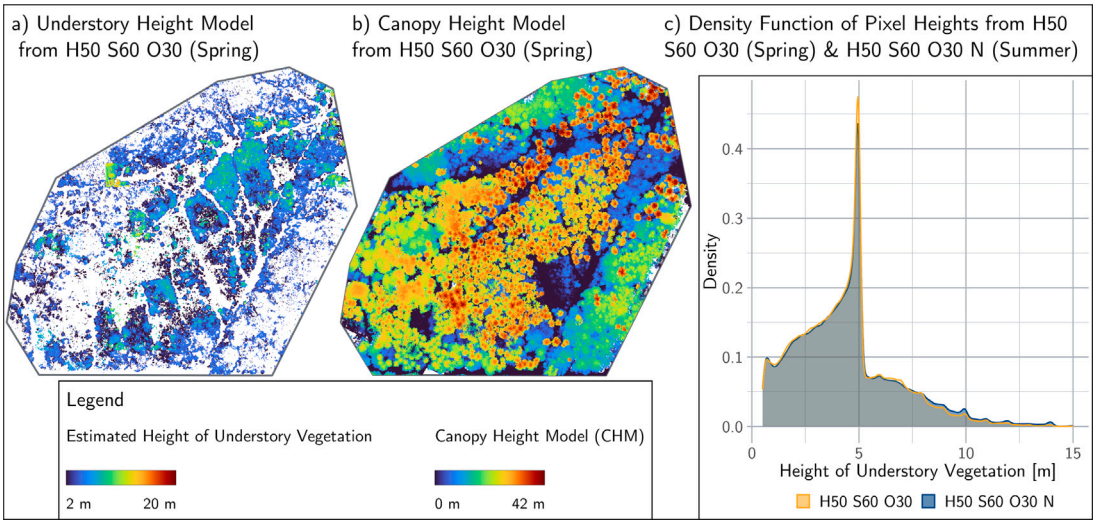

Fig. 8. Height of detected understory vegetation for flight parameter set H50 S60 O30 in spring (a), the corresponding canopy height map (b), and density function of pixel heights of the spring and summer data (c).

RMSE was found with the densely overlapped data (H50 S60 O60) with a recall rate of 86.7% and RMSE of 0.107 m over the for subsets, followed by the standard parameter set (H50 S60 O30) and the slowly flown data (H50 S40 O30) (compare table in Table A.2).

The results of the new algorithm have been compared with those achieved by the precursor algorithm of Neuville et al. (2021). We found an extremely low number of DBH estimates compared to our algorithm for the default parameters. If the estimation height segment was increased to 1 to 3 m and the starting minimum cluster size was reduced, the results improved, but were still worse than those obtained by our method. Beside its higher accuracy, the new algorithm was also more computationally efficient, with a computation time for the same dataset approx. one quarter lower as compared to the algorithm of Neuville et al. (2021). Note that it was not possible to compare how the same tree's DBH was estimated by both algorithms, as the number of remaining stems hit by both algorithms was too low. For our algorithm, no large differences in accuracy were observed between

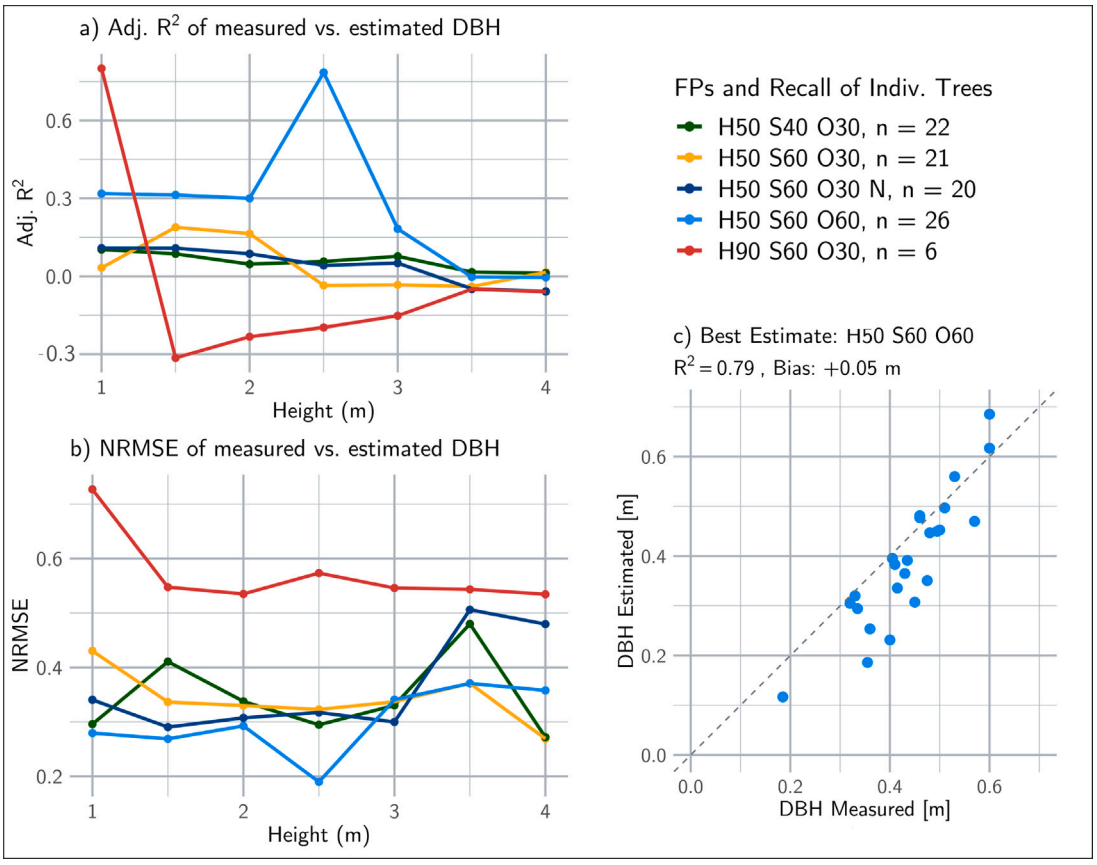

Fig. 9. Accuracy of DBH (diameter at breast height) estimation in relation to height of stem segments. For accuracy assessment, the adjusted R^2 (a) and normalised RMSE (b) values of the best estimation (highest adj. R^2, lowest NRMSE) between measured and estimated DBHs are presented. In the legend, n denotes the number of trees available for accuracy assessment. Additionally, the scatter plot for the best FP set (H50 S60 O60) of measured vs. estimated DBH values is shown (c). For the scatter plots based on the best estimate of the other FP sets, see Fig. A.3.

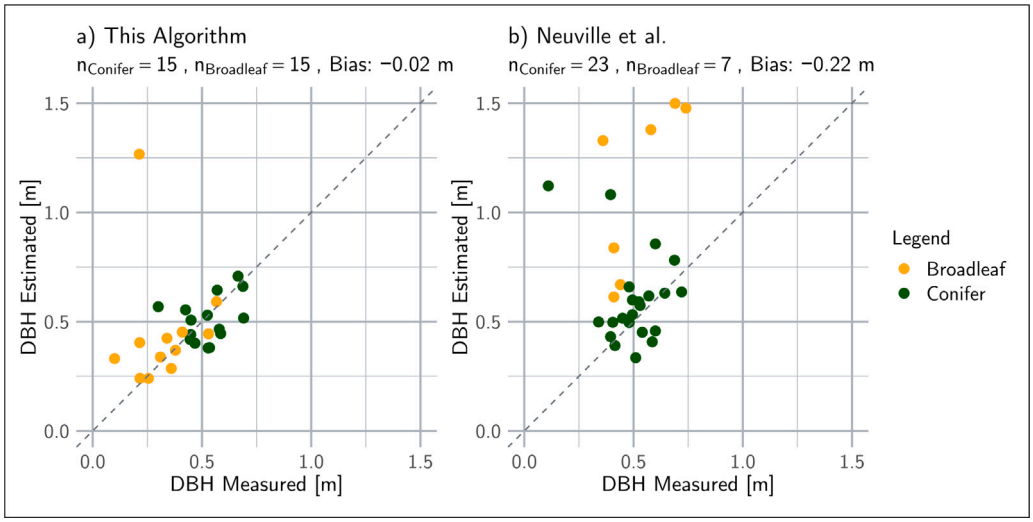

Fig. 10. Scatter plot of estimated vs. measured DBH (diameter at breast height) values from the validation set of stems for this algorithm (a) and Neuville et al. (2021) (b).

broadleaf and conifer trees. In contrast to the original method, only one single outlier was present (Fig. 10).

For the entire study area the DBH algorithm returned a total of 2723 DBH estimates (Fig. 11). On average, stems with a diameter of 28 cm were detected (Fig. 11b), with extremes up to 1.2 m and a recall of stems of 55%. Most of the detected stems belong to large trees in the upper canopy. However, stems of some smaller trees have also been detected with our algorithm. This is an advantage of the new algorithm, as the conditional selection of a single stem in each individual segmented tree in Neuville et al. (2021) inhibits the detection of stems in the lower canopy. Also noticeable is the lack of detected stems in the eastern and northern parts of the study area, which are dominated by broadleaf trees, highlighting the problem of lack of penetration below these canopies.

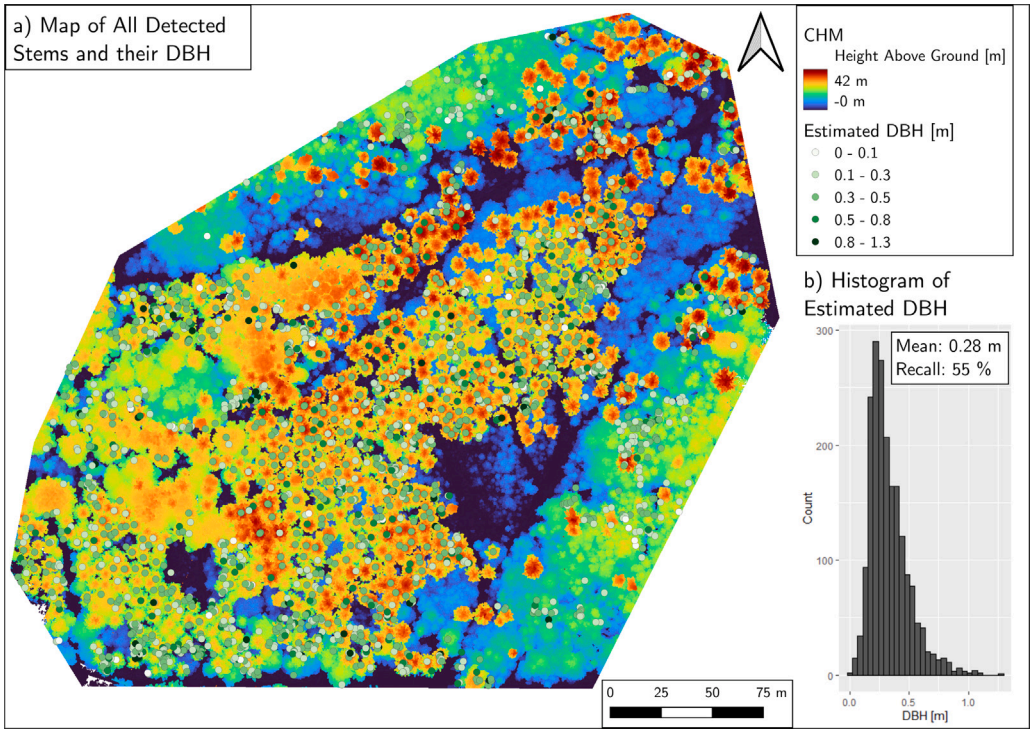

Fig. 11. Canopy height model (CHM) with positions and DBH (diameter at breast height) estimations overlaid, showing positions of detected stems and lack thereof in some regions of the forest (a). The corresponding histogram of DBH values is shown in (b).

4. Discussion

4.1. Flight parameters

The prerequisite for successfully estimating forest structural parameters from LiDAR is a sufficiently high density of LiDAR points from all relevant parts of the forest. Besides the choice of the LiDAR instrument, this is influenced by flight parameters such as flight height and speed. In this study, we provide the first systematic comparison of flight parameters and their effect on the usability of LiDAR data for stem detection in forests of varying structural complexity in tree stand density, species and presence of lower vegetation. As the LiDAR system used in this study is incapable of tilting, the investigation of these FP sets for stem point density is even more crucial, as the tilting is reliable method of increasing penetration to the stem of the tree (Neuville et al. 2021, Swayze et al. 2021).

Flight parameters influenced the usability of the data for stem detection, mainly by affecting point densities of LiDAR data in the understory vegetation and the lower stem segments of large trees, which also transferred to accuracy of DBH estimates. Irrespective of flight speed and overlap, a high flight height resulted in an insufficient number of return points at the tree stems for reliable detection (Fig. 3), while also exaggerating unwanted movement of the LiDAR in flight, due to the greater distance to the target. At 50 m flight height, a higher overlap of LiDAR stripes led to higher point densities in the stem segment compared to reduced flight speed, if all other parameters are kept the same. Consequently, the best data was collected with a FP set of low height, high overlap and a relatively high flight speed (Fig. 3). The stronger influence of overlap on the point densities of the stems compared to a reduced flight speed can be explained by a higher overlap, which increases the observing positions of the LiDAR device over the forest. This boosts the chance for gaps in the canopy where the LiDAR beam can penetrate, thus increasing the number of return points at the lower stem segments (Fig. 3).

Another advantage for the higher overlap is the drone's position in flight. Neuville et al. (2021), and Feng et al. (2022), among others, have shown that a tilted LiDAR will outperform a straight nadir-looking one for stem remote sensing, as it allows one to somewhat look underneath the tree's canopy. A reduced effect of this 'tilting' can be seen by the impact of flight speed, as the measurement setup used here features no gimbal: The higher the drone's speed, the further it has to pitch in the flight direction, which tilts the LiDAR with it. This might further explain the slightly improved performance under higher flight speeds, giving better results for the DBH estimation under the standard FP set (H50 S60 O30), compared to the slower flown FP set (H50 S40 O30).

LiDAR as an active system can be flown at night, which should theoretically reduce random back-scatter caused by sunlight. However, in our data, lower point densities and an only slightly increased accuracy were observed for nighttime data compared to daytime data, when sharing the same FP set. Here, it should be noted that the differences in accuracy might also be influenced by the phenological difference in data acquisition between day- and nighttime data. Therefore, nighttime data appears to be advantageous only due to the presence of less turbulent air, which disturbs the drone less in flight, caused by a more stratified atmosphere (Stull, 1988). Lastly, a denser point cloud at canopy level has been found for higher flight heights, while lower flight heights led to higher numbers of points in the stem segment. Consequently, the optimal FP set must be chosen considering the specific research questions and no general advice for LiDAR data acquisition in temperate forests can be given.

4.2. Stem delineation algorithms

The new approach is capable of robustly detecting stem points within the point cloud, with a good stem recall in most areas. The delineation fails for smaller trees, especially if the number of stem points is low beneath a closed canopy of major broadleaf trees.

The algorithm struggles with trees presenting unusual growing directions (i.e. growing extremely askew, branching out at low height and at a shallow angle, or being very gnarled), caused by the definition of stems as upwards spread clusters. However, compared to the original method by Neuville et al., our algorithm segmented branching stems, if they grow mainly upwards, which is not possible in the original method per definition of a single stem per tree. If trees with unusual growing direction dominate a study area such as in non-managed forests, the algorithm's parameters (PCA threshold, maximum height of stem) can be changed to improve results.

Compared to the TreeLS algorithm, the new method achieves an overall higher recall and more accurate stem segmentation, even when TreeLS's parameters were adapted to the study site. However, it should be noted that TreeLS is primarily designed for TLS and not ALS data. As ALS data's geolocation is typically less accurate than that of TLS data (Brede et al., 2017), the noise in geolocation might cause the method to be less applicable for searching horizontal circles in the data to detect stems, at least for this study area and the ALS used. On the other hand, we expect the newly designed algorithm to be adaptable for other study sites and LiDAR-systems, not just ALS, but also TLS or portable LiDAR systems (PLS, Parker et al., 2004).

Another reason for the comparably bad performance of TreeLS's algorithm is likely the LiDAR's lack of penetration through the canopy to the stem. This causes many tree stems to be detected only from one side. We assume that this is the reason that some stems do not appear as cylinders but as ellipses or curved lines, when observed from above (Fig. 7). As a result, a substantial number of stems is simply disregarded, as the Hough-transformation does not find circles there.

4.3. Understory detection

The understory vegetation detection worked well independent of forest structure and led to clear patches of different understory vegetation heights and densities. In addition, areas without understory vegetation can be detected, unable to be seen from canopy maps or RGB-imagery. However, due to cell-wise calculation of breakpoints, some artefacts occurred, especially at the border of adjacent cells. A smaller cell-size might reduce this issue, but reduces points for the density calculation and requires significantly more computation time. The noticeable spike in the data at low vegetation heights (Fig. 8) is likely caused by more returns from grasses and lower shrubs, which the LiDAR cannot reach in summer, due to the denser foliage above these plants. Previous studies from Wing et al. (2012) and Venier et al. (2019) showed the possibilities of ALS data for the detection and analysis of understory vegetation. However, both methods did not solely rely on LiDAR data but instead required intensive field work to accurately observe the validity of their methods or developed models for the estimation of low vegetation. It should be noted that our method relies on a definite break point in vertical point densities between understory and canopy vegetation, which is only present if the forest consists of vertical layers. For such forests, which are a common sight under current forest management, this method makes it possible to quickly approximate the height and state of the understory vegetation. However, using only ALS data, a classification of detected understory vegetation into small trees, shrubs, and grasses is hardly possible.

4.4. DBH-estimation

The DBH estimation using our approach was similarly accurate compared to previous studies with more costly LiDAR equipment (Neuville et al., 2021, Brede et al., 2017, Feng et al., 2022). We applied the approaches of the previous studies to our data and found that our algorithm outperformed the previous ones regarding the number of stems detected in the forest and the accuracy of stem diameter estimation. The newly developed method outperformed the existing one in our study area, especially regarding the lower number of outliers. Such outliers are likely caused by the failure of the circle fit for the diameter estimation, which the method of Neuville et al. (2021) relies on, potentially leading to an overestimation of DBH values. Especially broadleaf trees are not accurately estimated by the original method, likely due to fewer points in the stem segment, making a reliable circle fit hardly possible. A similar tendency of producing outliers of overestimation could also be seen in the results of Neuville et al. (2021). Furthermore, their set maximum value of plausible DBH of 1.5 m did remove numerous values altogether (Neuville et al., 2021). On the other hand, the new algorithm revealed good performance irrespective of tree species, as seen from the results of the broadleaf-dominated subplot (Table A.2) or the validation of DBH accuracy by tree species (Fig. 10), which showed similar performance in recall and accuracy when comparing broadleaf and conifer dominated subplots or broadleaf and conifer trees.

For the newly developed algorithm, we found the highest accuracy of DBH estimation from an extraction height of 2.5 m above ground ± 0.5 m, which is caused by less understory vegetation and little change of stem diameter compared to 1.3 m above ground (Pukkala et al., 2019), while also including enough points. Using these algorithm parameters and FP set did also show the best results over the four subplots, highlighting the usability irregardless of forest characteristics in terms of tree species, presence of understory vegetation and stand density. The relatively low quantile of distances for the estimation (80 %) further hints at the lack of accuracy of the LiDAR used, as the stem's diameter should reduce at 2.5 m height compared to 1.3 m. As this inaccuracy of the LiDAR could be seen with the example stem shapes (Fig. 7), this is likely not due to an inaccurate segmentation of stems, but the LiDAR scanner itself.

The differences in accuracy between the densely overlapped and the other FP sets cannot be fully explained. At higher flight height, small movements of the drone can be amplified, yet these differences also occur within the flights' data conducted at the same flight height. This leaves the conclusion that the presented algorithm does allow for the best results in terms of accuracy and recall, when there are more points in the stem segment.

Since this approach has the advantage of being much faster than previous methods, especially those using TLS data, the algorithm can be applied to large forest areas. Compared to the method by Neuville et al. (2021), substantially faster calculation times could be observed (especially when using DBSCAN for the initial and secondary step of clustering).

5. Conclusion and suggestions

In this study, we tested for the first time how FP sets for drone-based LiDAR acquisitions affect the detection of understory vegetation and stems of major trees below dense canopy. We found that the selection of FPs, especially flight height, must be adapted to the research focus, with higher flight heights performing better if the canopy or ground are of interest and lower flight heights if stems are the main focus (Fig. 3). Even though the accuracy of DBH estimates were found to depend on the FP set, we could not determine the exact cause, albeit a positive correlation between point density at stem segment and DBH estimation accuracy and recall was detected. Taken together with the limited flight time of UAVs, we, therefore, suggest using a denser overlap of flight stripes to achieve this point density. We also tested two existing approaches for the detection of stems and estimation of stem diameters against a newly developed algorithm in different forest stands. Compared to the other approaches, our newly developed approach improved computational efficiency and accuracy in estimates, with lowered differences in accuracy depending on tree species. We therefore conclude that the new algorithm used with suitable LiDAR data should be considered in future studies if stem properties or classification of understory vegetation in structurally complex forests are targeted, using the DBSCAN algorithm for both clustering steps, if the

study area is large. Depending on the site to be analysed, this new algorithm can easily be adapted to local conditions.

With the limitations and possibilities mentioned above, we advocate for airborne LiDAR scanning as the only feasible method to generate 3D point clouds in large forest areas. Both terrestrial and portable laser scanning could lead to denser point clouds in the stem segment, with the latter also increasing accuracy (Torralba et al., 2022). However, especially the recording of TLS data can be very time-consuming, even taking multiple days depending on forest structure for a single hectare (Wilkes et al., 2017) and is considerably harder to perform depending on the presence of understory vegetation (Åkerblom and Kaitaniemi, 2021). Consequently, slightly higher data accuracy and higher point density in the stem segment do not merit time-intensive and more complex data recording and leave ALS as the only feasible method. Further work could investigate whether LiDAR data acquired in winter could minimise the effect of understory vegetation for stem segmentation and DBH-estimation, especially in broadleaf-dominated forests. Furthermore, the effects of a tilted LiDAR using a 3D printed mounting system to increase the recall of stems and diameter estimates by increasing points in the stem segment could be investigated. Lastly, the accuracy of stem segmentation could be increased by choosing different algorithm parameters depending on tree stand age, approximated by tree height.

For forester practice, we expect that the delineation of stems together with estimation of DBH will be helpful, as it provides important information about current forest value and value changes over time. Combined with information about tree species, this could be used to approximate the economical value of the entire forest area on an individual tree scale. In addition, information about understory vegetation and terrain could be used to predict the expenses of harvesting itself. This proposed methodology provides a relatively inexpensive, fast and easy-to-implement tool for foresters to make timely decisions solely based on UAV LiDAR and RGB remote sensing.

CRediT authorship contribution statement

Paul M. Eisenschink: Writing – original draft, Methodology, Investigation, Conceptualization. **Wolfgang A. Obermeier:** Writing – review & editing, Visualization, Project administration. **Vinzenz H.D. Zerres:** Writing – review & editing, Visualization, Investigation. **Annika M. Suerbaum:** Writing – review & editing, Investigation. **Lukas W. Lehnert:** Writing – original draft, Supervision, Project administration, Conceptualization.

Funding

This study was funded under the LabForest project by the Bundesministerium für Bildung und Forschung (German federal ministry of education and research, BMBF), Bonn, Germany [grant number 033L307A].

Declaration of competing interest

The authors declare that they have no known competing financial interests or personal relationships that could have appeared to influence the work reported in this paper.

Appendix

See Figs. A.1–A.3.

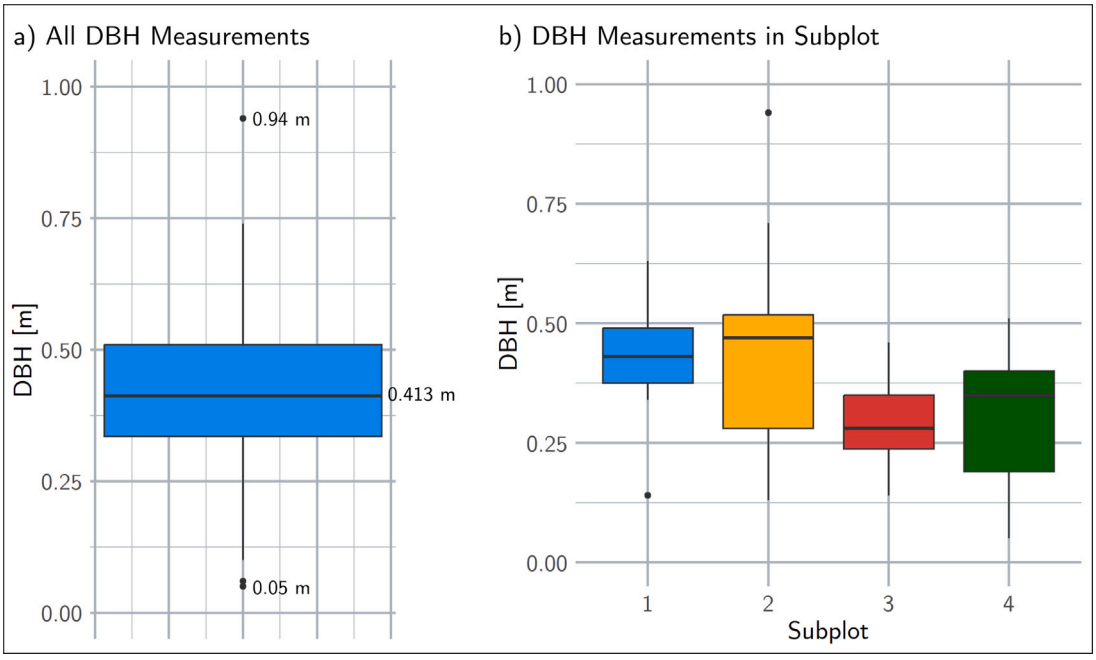

Fig. A.1. Box plot of measured DBH (diameter at breast height) values for training/validation with extremes and median (a) and box plots of measured DBH-values per subplot (b). The four subplots consist of old-growth conifers (spruce and pine) both with little to no advanced regeneration (1), very dense advanced regeneration of beech up to 10 m in height (2), old-growth broadleaf trees (oak, beech, and maple) with decent advanced regeneration (3), and younger coniferous trees (4).

Table A.2
Table of metrics for point cloud metrics, stem delineation, diameter at breast height (DBH) estimation for the five main flight parameter (FP) sets and the four chosen subplots.

FP Set	H50 S60 060	H50 S60 O30	H50 S60 O30 N	H90 S60 O30	H50 S40 O30
Avg. Point Density [Pts/m]	4177	2429	2423	1011	2609
Stems Visible	34/34/8/29	29/26/7/26	28/31/6/26	26/18/2/9	28/22/4/25
Sum Stems Visible	105	88	91	55	79
Recall Stems per SP	31/26/6/28	20/17/4/21	18/23/3/23	19/10/0/3	21/17/2/20
Sum Stems	91	62	59	32	60
Recall Stems [%]	86.7	70.5	64.8	58.2	75.9
RMSE DBH per SP [m]	0.078/0.134/0.103/0.049	0.122/0.100/0.199/0.123	0.150/0.104/0.287/0.164	0.110/0.155/NA/NA	0.141/0.139/0.001/0.099
RMSE DBH Total [m]	0.107	0.129	0.16	0.147	0.136
Recall DBH per SP	10/12/5/2	9/10/4/3	12/9/3/1	2/8/0/0	11/11/1/1
Recall Total	29	26	25	10	24
Recall Stems TreeLS	24/17/0/18				
Sum Stems TreeLS	59				
Recall TreeLS [%]	56.2				

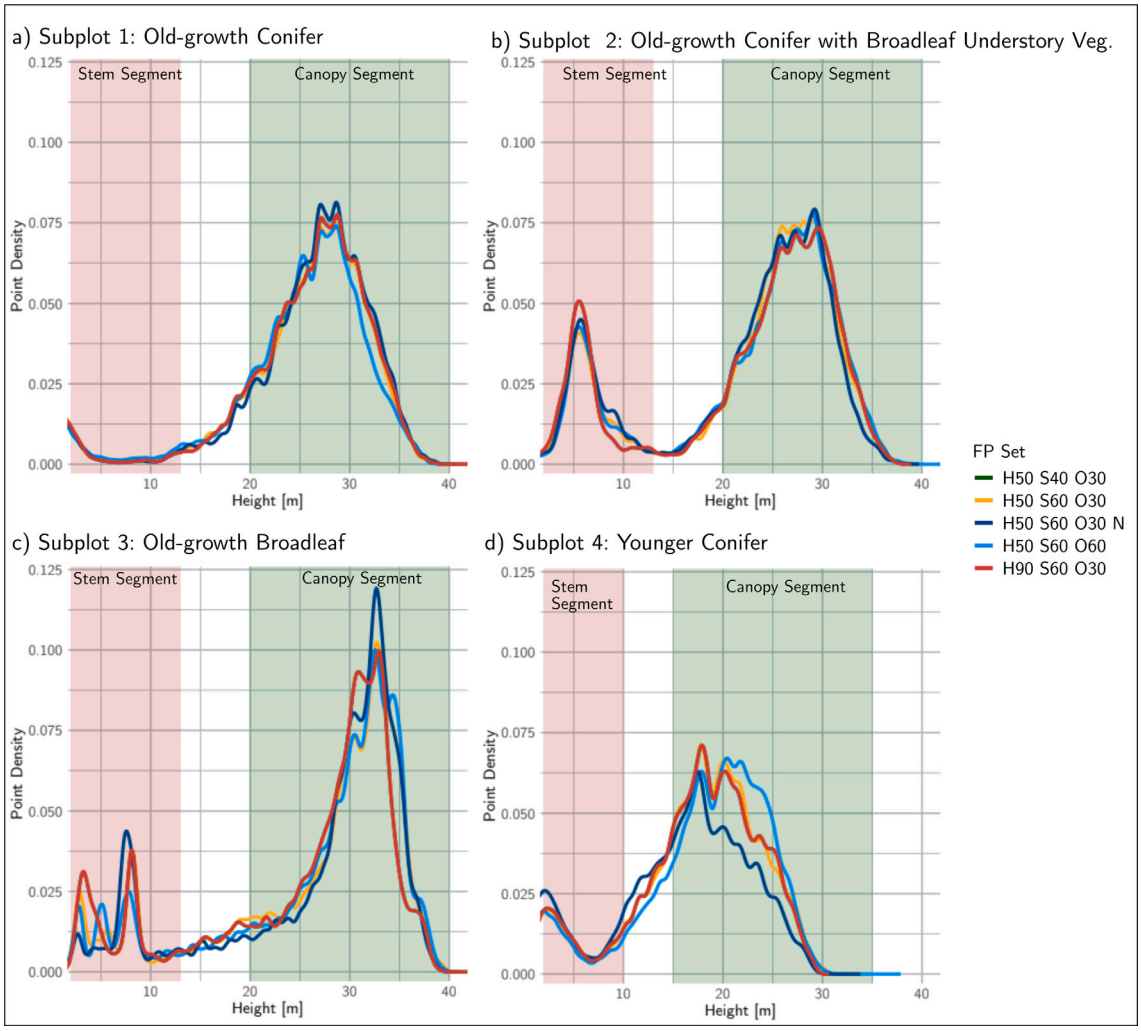

Fig. A.2. Point density distribution over the four subplots and five flight parameter (FP) sets.

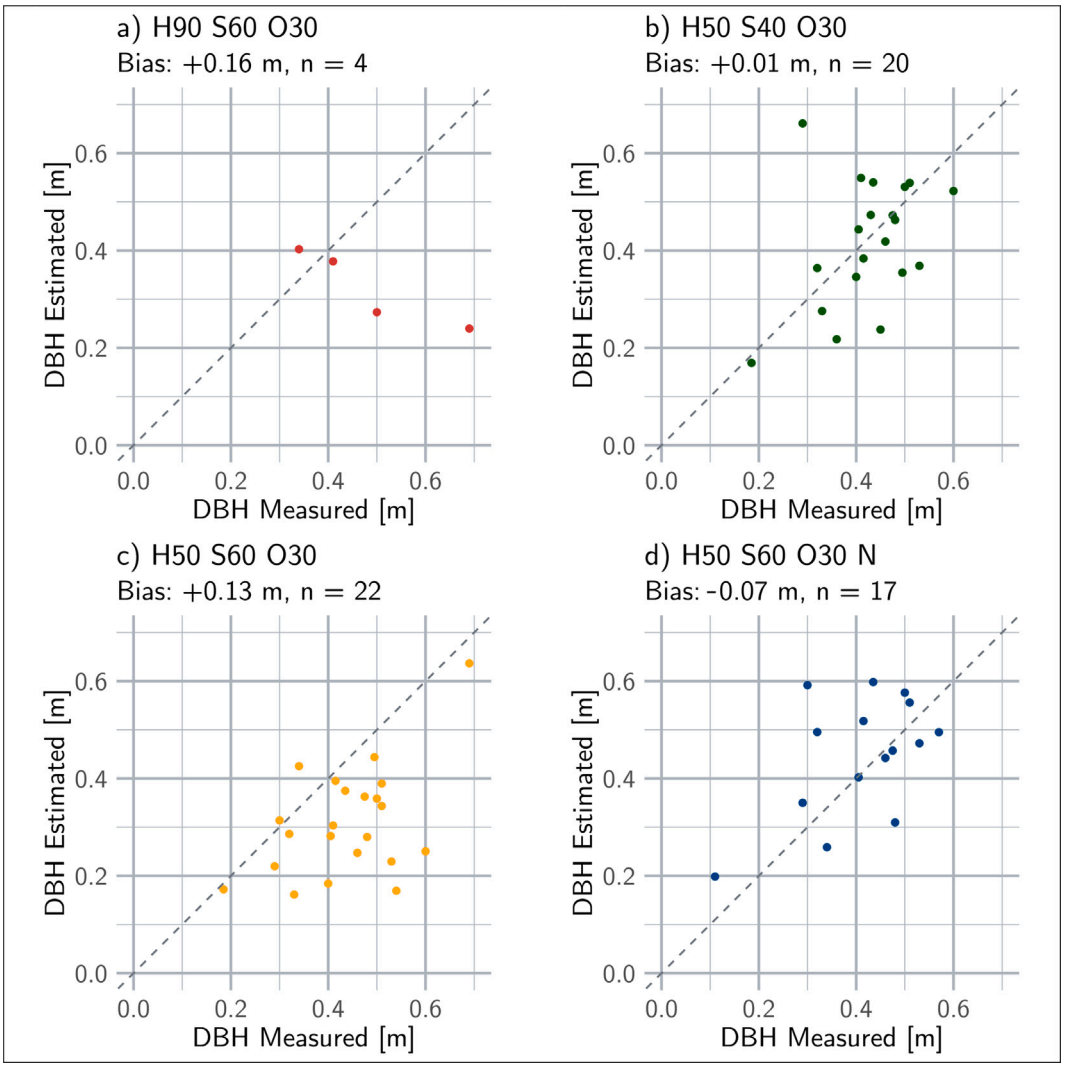

Fig. A.3. Scatter plots of estimated vs. measured diameter at breast height (DBH) for the best algorithm parameter settings for the remaining four flight parameter sets. Differences in number estimated stems is caused by recall of the DBH algorithm.

Data availability

The five mainly used LiDAR-datasets as well as the code used for the methods can be found under https://data.mendeley.com/datasets/5fjwb9hfpm/1. Due to file-size constrains the remaining three LiDAR datasets will be made available on request.

References

Åkerblom, M., Kaitaniemi, P., 2021. Terrestrial laser scanning: a new standard of forest measuring and modelling? Ann. Botany 128 (6), 653–662. http://dx.doi.org/10.1093/aob/mcab111.

Brandl, S., Paul, C., Knoke, T., Falk, W., 2020. The influence of climate and management on survival probability for Germany's most important tree species. For. Ecol. Manag. 458 (117652), 117652. http://dx.doi.org/10.1016/j.foreco.2019.117652.

Brede, B., Lau, A., Bartholomeus, H., Kooistra, L., 2017. Comparing RIEGL RiCOPTER UAV LiDAR derived canopy height and DBH with terrestrial LiDAR. Sensors (Basel) 17 (10), 2371. http://dx.doi.org/10.3390/s17102371.

Brockerhoff, E.G., et al., 2017. Forest biodiversity, ecosystem functioning and the provision of ecosystem services. Biodivers. Conserv. 26 (13), 3005–3035. http://dx.doi.org/10.1007/s10531-017-1453-2.

Campbell, J.B., Wynne, R.H., 2011. Introduction to remote sensing, fifth edition, fifth ed. Guilford Publications, New York, NY.

Campello, R.J.G.B., Moulavi, D., Sander, J., 2013. Density-based clustering based on hierarchical density estimates. In: Advances in Knowledge Discovery and Data Mining. Springer Berlin Heidelberg, pp. 160–172. http://dx.doi.org/10.1007/978-3-642-37456-2_14.

Caudullo, G., Tinner, W., de Rigo, D., 2016. Picea abies in europe: distribution, habitat, usage and threats. In: n San-Miguel-Ayanz, J., de Rigo, D., Caudullo, G., Durrant, T.H., Mauri, A. (Eds.), European Atlas of Forest Tree Species. Publications Office of the European Union, Luxembourg, http://dx.doi.org/10.7892/boris.80794.

Chisholm, R.A., Cui, J., Lum, S.K.Y., Chen, B.M., 2013. UAV LiDAR for below-canopy forest surveys. J. Unmanned Veh. Syst. 01 (01), 61–68. http://dx.doi.org/10.1139/juvs-2013-0017.

Corte, D., et al., 2020. Measuring individual tree diameter and height using GatorEye high-density UAV-lidar in an integrated crop-livestock-forest system. Remote. Sens. 12 (5), 863. http://dx.doi.org/10.3390/rs12050863.

de Conto, T., 2020. TreeLS: Terrestrial point cloud processing of forest data. URL https://CRAN.R-project.org/package=TreeLS R package version 2.0.2.

de Conto, T., Olofsson, K., Görgens, E.B., Rodriguez, L.C.E., Almeida, G., 2017. Performance of stem denoising and stem modelling algorithms on single tree point clouds from terrestrial laser scanning. Comput. Electron. Agric. 143, 165–176. http://dx.doi.org/10.1016/j.compag.2017.10.019.

de Conto, T., Roussel, J.-R., Hamamura, C., Marcozzi, A., 2021. TreeLS Forest structure reconstruction from LiDAR data. R package version 1.3.0 https://github.com/tiagodc/TreeLS.

Deutscher Wetterdienst (DWD), 2024. Climate data: Multi-annual means 1991–2020. URL https://opendata.dwd.de/climate_environment/CDC/observations_germany/climate/multi_annual/mean_91-20/ (Accessed: 20 Nov 2024).

Dyderski, M.K., Paź, S., Frelich, L.E., Jagodziński, A.M., 2018. How much does climate change threaten European forest tree species distributions? Glob. Chang. Biol. 24 (3), 1150–1163. http://dx.doi.org/10.1111/gcb.13925.

Ester, M., Kriegel, H.-P., Sander, J., Xu, X., 1996. A density-based algorithm for discovering clusters in large spatial databases with noise. In: Proceedings of the Second International Conference on Knowledge Discovery and Data Mining. KDD '96, AAAI Press, pp. 226–231. http://dx.doi.org/10.5555/3001460.3001507, URL https://www.dbs.ifi.lmu.de/Publikationen/Papers/KDD-96.final.frame.pdf.

Fahey, T.J., Woodbury, P.B., Battles, J.J., Goodale, C.L., Hamburg, S.P., Ollinger, S.V., Woodall, C.W., 2009. Forest carbon storage: ecology, management, and policy. Front. Ecol. Environ. 8 (5), 245–252. http://dx.doi.org/10.1890/080169.

Feng, B., Nie, S., Wang, C., Xi, X., Wang, J., Zhou, G., Wang, H., 2022. Exploring the potential of UAV LiDAR data for trunk point extraction and direct DBH measurement. Remote. Sens. (Basel) 14 (12), 2753. http://dx.doi.org/10.3390/rs14122753.

Ferraz, A., Saatchi, S., Mallet, C., Meyer, V., 2016. Lidar detection of individual tree size in tropical forests. Remote Sens. Environ. 183, 318–333. http://dx.doi.org/10.1016/j.rse.2016.05.028.

Huang, S., Krysanova, V., Hattermann, F., 2015. Projections of climate change impacts on floods and droughts in Germany using an ensemble of climate change scenarios. Reg. Env. Chang. 15 (3), 461–473. http://dx.doi.org/10.1007/s10113-014-0606-z.

Jeronimo, S.M.A., Kane, V.R., Churchill, D.J., McGaughey, R.J., Franklin, J.F., 2018. Applying LiDAR individual tree detection to management of structurally diverse forest landscapes. J. For. 116 (4), 336–346. http://dx.doi.org/10.1093/jofore/fvy023, arXiv:https://academic.oup.com/jof/article-pdf/116/4/336/25106382/fvy023.pdf.

Kloos, S., Yuan, Y., Castelli, M., Menzel, A., 2021. Agricultural drought detection with MODIS based vegetation health indices in southeast Germany. Remote. Sens. (Basel) 13 (19), 3907. http://dx.doi.org/10.3390/rs13193907.

Liao, K., Li, Y., Zou, B., Li, D., Lu, D., 2022. Examining the role of UAV lidar data in improving tree volume calculation accuracy. Remote. Sens. (Basel) 14 (17), 4410. http://dx.doi.org/10.3390/rs14174410.

Neuville, R., Bates, J.S., Jonard, F., 2021. Estimating forest structure from UAV-mounted LiDAR point cloud using machine learning. Remote. Sens. (Basel) 13 (3), 352. http://dx.doi.org/10.3390/rs13030352.

Parker, G.G., Harding, D.J., Berger, M.L., 2004. A portable LIDAR system for rapid determination of forest canopy structure. J. Appl. Ecol. 41 (4), 755–767. http://dx.doi.org/10.1111/j.0021-8901.2004.00925.x.

Poschlod, B., Willkofer, F., Ludwig, R., 2020. Impact of climate change on the hydrological regimes in bavaria. Water (Basel) 12 (6), 1599. http://dx.doi.org/10.3390/w12061599.

Pukkala, T., Hanssen, K., Andreassen, K., 2019. Stem taper and bark functions for Norway spruce in Norway. Silva Fenn. 53 (3), http://dx.doi.org/10.14214/sf.10187.

Pyhäjärvi, T., Kujala, S.T., Savolainen, O., 2019. 275 years of forestry meets genomics inpinus sylvestris. Evol. Appl. 13 (1), 11–30. http://dx.doi.org/10.1111/eva.12809.

Roussel, J.-R., et al., 2020. lidR: An r package for analysis of airborne laser scanning (ALS) data. Remote Sens. Environ. 251, 112061. http://dx.doi.org/10.1016/j.rse.2020.112061.

Singh, A., Kushwaha, S.K.P., Nandy, S., Padalia, H., 2022. An approach for tree volume estimation using RANSAC and RHT algorithms from TLS dataset. Appl. Geomatics 14 (4), 785–794. http://dx.doi.org/10.1007/s12518-022-00471-x.

Spinoni, J., Vogt, J.V., Naumann, G., Barbosa, P., Dosio, A., 2018. Will drought events become more frequent and severe in europe? Int. J. Climatol. 38 (4), 1718–1736. http://dx.doi.org/10.1002/joc.5291.

Stull, R.B., 1988. An Introduction to Boundary Layer Meteorology. Springer Netherlands, http://dx.doi.org/10.1007/978-94-009-3027-8.

Swayze, N.C., Tinkham, W.T., Vogeler, J.C., Hudak, A.T., 2021. Influence of flight parameters on UAS-based monitoring of tree height, diameter, and density. Remote Sens. Environ. 263, 112540. http://dx.doi.org/10.1016/j.rse.2021.112540.

Ter-Mikaelian, M.T., Korzukhin, M.D., 1997. Biomass equations for sixty-five North American tree species. Forest Ecol. Manag. 97 (1), 1–24. http://dx.doi.org/10.1016/s0378-1127(97)00019-4.

Thonfeld, F., Gessner, U., Holzwarth, S., Kriese, J., da Ponte, E., Huth, J., Kuenzer, C., 2022. A first assessment of canopy cover loss in Germany's forests after the 2018–2020 drought years. Remote. Sens. (Basel) 14 (3), 562. http://dx.doi.org/10.3390/rs14030562.

Torralba, J., Carbonell-Rivera, J.P., Ruiz, L.A., Crespo-Peremarch, P., 2022. Analyzing TLS scan distribution and point density for the estimation of forest stand structural parameters. Forests 13 (12), 2115. http://dx.doi.org/10.3390/f13122115.

Venier, L.A., Swystun, T., Mazerolle, M.J., Kreutzweiser, D.P., Wainio-Keizer, K.L., McIlwrick, K.A., Woods, M.E., Wang, X., 2019. Modelling vegetation understory cover using LiDAR metrics. In: Van Stan, J.T. (Ed.), PLOS ONE 14 (11), http://dx.doi.org/10.1371/journal.pone.0220096.

Wilkes, P., et al., 2017. Data acquisition considerations for terrestrial laser scanning of forest plots. Remote Sens. Environ. 196, 140–153. http://dx.doi.org/10.1016/j.rse.2017.04.030.

Wing, B.M., Ritchie, M.W., Boston, K., Cohen, W.B., Gitelman, A., Olsen, M.J., 2012. Prediction of understory vegetation cover with airborne lidar in an interior ponderosa pine forest. Remote Sens. Environ. 124, 730–741. http://dx.doi.org/10.1016/j.rse.2012.06.024.

Zhang, Q., Li, Y., Yu, C., Qi, J., Yang, C., Cheng, B., Liang, S., 2020. Global timber harvest footprints of nations and virtual timber trade flows. J. Clean. Prod. 250, 119503. http://dx.doi.org/10.1016/j.jclepro.2019.119503.

Zhang, W., Qi, J., Wan, P., Wang, H., Xie, D., Wang, X., Yan, G., 2016. An easy-to-use airborne LiDAR data filtering method based on cloth simulation. Remote. Sens. 8 (6), 501. http://dx.doi.org/10.3390/rs8060501.